Two-Dimensional Beam Steering Using an Electrically Tunable Impedance Surface

Daniel F. Sievenpiper, *Member, IEEE*, James H. Schaffner, *Senior Member, IEEE*, H. Jae Song, *Member, IEEE*, Robert Y. Loo, *Member, IEEE*, and Gregory Tangonan, *Member, IEEE*

***Abstract*—By covering a metal ground plane with a periodic surface texture, we can alter its electromagnetic properties. The impedance of this metasurface can be modeled as a parallel resonant circuit, with sheet inductance L, and sheet capacitance C. The reflection phase varies with frequency from $+\pi$ to $-\pi$, and crosses through 0 at the *LC* resonance frequency, where the surface behaves as an artificial magnetic conductor. By incorporating varactor diodes into the texture, we have built a tunable impedance surface, in which an applied bias voltage controls the resonance frequency, and the reflection phase. We can program the surface to create a tunable phase gradient, which can electronically steer a reflected beam over +/− 40° in two dimensions, for both polarizations. We have also found that this type of resonant surface texture can provide greater bandwidth than conventional reflectarray structures. This new electronically steerable reflector offers a low-cost alternative to a conventional phased array.**

***Index Terms*—Antenna arrays, grid arrays, high impedance surfaces, impedance sheets, reconfigurable antennas, scanning antennas, textured surfaces, tunable antennas.**

I. Introduction

It is well-known that metal-dielectric composite textures can be used to alter the electromagnetic properties of metal surfaces to perform a variety of functions. For example, specific textures can be designed to change the surface impedance for one or both polarizations, or to manipulate the propagation of surface waves. The simplest examples are corrugated metal sheets, often known as soft and hard surfaces. [1] These materials are typically built as a metal slab with quarter-wavelength deep corrugations. They are usually analyzed by treating the corrugations as quarter-wavelength transmission lines, in which the short circuit at the bottom of each groove is transformed into an open circuit at the top surface. This provides a high-impedance boundary condition for electric fields polarized perpendicular to the corrugations, and low-impedance for electric fields parallel to the grooves. Soft and hard surfaces are used in various applications such as manipulating the radiation patterns of horn antennas, or controlling the edge diffraction of reflectors. Further background on these and related structures can be found in the literature on corrugated surfaces [2]–[6]. Similar structures have also been built in two dimensions, such as two-dimensional (2-D) shorted waveguide arrays [7], or the inverse structures, which are known as pin-bed surfaces [8]. These textured materials are typically one-quarter wavelength thick in order to achieve a high-impedance boundary condition.

Recently, compact structures have been developed that can also alter the electromagnetic boundary condition of a metal surface, but which are much less than one-quarter wavelength thick. The reduction in thickness is achieved by capacitive loading, such as by using closely spaced mushroom-shaped metal protrusions, or overlapping thumbtack-like structures [9], [10]. These materials provide a high-impedance boundary condition ($Z_s \gg 377\ \Omega$) for both polarizations. They are sometimes known as artificial magnetic conductors, because the tangential magnetic field is zero at the surface, rather than the electric field, as with an ordinary metal. In addition to their unusual reflection phase properties, these materials have a surface wave bandgap, within which they do not support bound surface waves of either TM or TE polarization. However, they do support leaky TE waves, which can be useful for certain applications. The surface wave properties of these materials are described in greater detail elsewhere [9], [10]. In the present paper, we are only interested in their reflection phase properties, which are the basis of our electronically steerable reflector.

Conventional high-impedance surfaces are typically constructed as printed circuit boards, where the bottom side is a solid metal ground plane, and the top contains an array of small ($\ll \lambda$) metal patches The plates are connected to the ground plane by metal plated vias to form a continuous textured metal structure. An example of such a material is shown in Fig. 1. It can be considered as a 2-D version of the corrugated ground plane, where the quarter-wavelength resonant corrugations have been folded up into small resonant circuits, and distributed on a 2-D lattice.

When the period is small compared to the wavelength of interest, we may analyze the material as an effective medium, with its surface impedance defined by effective lumped-element circuit parameters that are determined by the geometry of the surface texture. A wave impinging on the material causes electric fields to span the narrow gaps between the neighboring metal patches, and this can be described as a sheet capacitance C, with units of [$\mathrm{Farads} * \mathrm{square}$]. As currents oscillate between the neighboring patches, the conducting paths through the vias and the ground plane provide a sheet inductance L, with units of [Henrys/square]. These form a parallel resonant circuit that dictates the electromagnetic behavior of the material. Its surface impedance is given by

$$Z_s = \frac{j\omega L}{1-\omega^2 LC}. \tag{1}$$

Manuscript received September 30, 2002; revised January 22, 2003. This work was supported in part by DARPA under Contract N6601-99-C-8635.

D. F. Sievenpiper, J. H. Schaffner, and H. J. Song are with HRL Laboratories LLC, Malibu, CA 90265 USA.

R. Loo was with retired from HRL Laboratories LLC, Malibu, CA 90265 USA. He is now with Wireless MEMS Incorporated, Oak Park, CA 91377 USA.

G. Tangonan was with HRL Laboratories LLC, Malibu, CA 90265 USA. He is now with the Ateneo de Manila University, Quezon City, Philippines.

Digital Object Identifier 10.1109/TAP.2003.817558

0018-926X/03$17.00 © 2003 IEEE

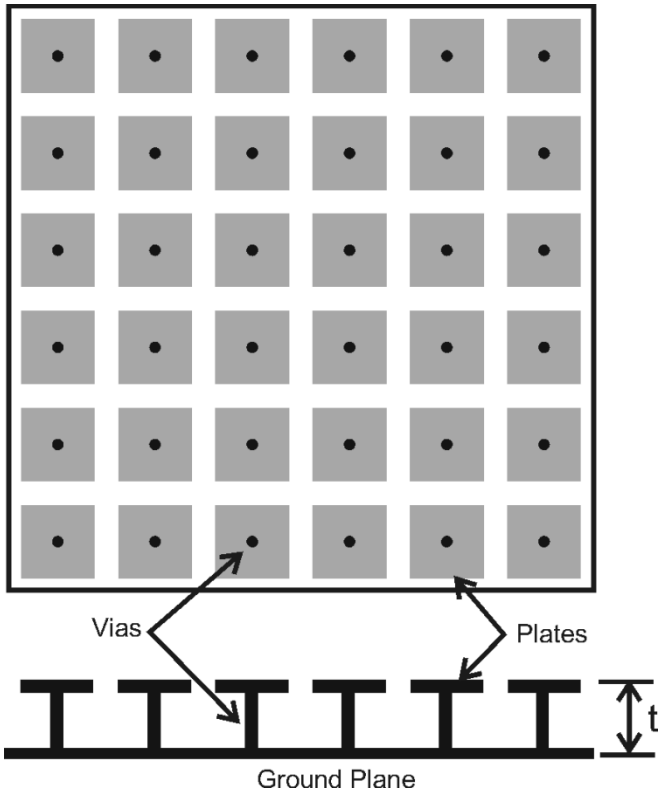

Fig. 1. Resonant textured surface, that is the basis of our 2-D beam steering reflector. It is constructed as a printed circuit board, where metal plated vias connect an array of plates on the top surface to a metal ground plane on the bottom surface. The capacitance and inductance between the plates determine the electromagnetic properties of the surface.

The surface impedance becomes infinite at the resonance frequency, which is

$$\omega_0 = \frac{1}{\sqrt{\mathrm{LC}}}. \tag{2}$$

For a normally incident wave, the reflection phase of the surface is

$$\phi = \mathrm{Im}\left\{\mathrm{Ln}\left(\frac{Z_s - \eta}{Z_s + \eta}\right)\right\} \tag{3}$$

where $\eta = 377\,\Omega$ is the impedance of free space. This reflection phase function is shown in Fig. 2.

Far below the resonance frequency, the surface reflects with a phase shift of π, just like an ordinary electric conductor. The reflection phase decreases with higher frequencies, crossing through 0 at resonance, where the surface behaves as an artificial magnetic conductor, and approaches $-\pi$ for frequencies far above resonance. Applications for these surfaces include low-profile antennas, in which radiating elements can lie very close ($\ll \lambda$) to a high-impedance ground plane without being shorted out. The effective image currents in an artificial magnetic conductor are in-phase with the antenna current, and thus reinforce the radiation, rather than canceling it as with an electric conductor.

The effective surface impedance model is not strictly valid for objects that are much closer than a wavelength from the surface. However, we find that in practice, antennas can be built as close as 1/100 wavelength from a properly designed textured surface

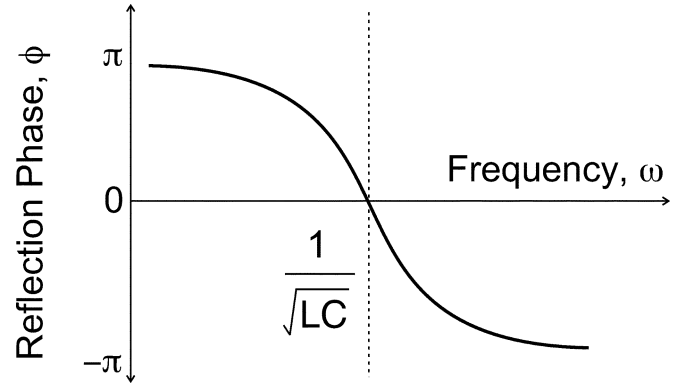

Fig. 2. Reflection phase of a resonant textured surface crosses through 0 at the resonance frequency, where the surface behaves as an artificial magnetic conductor. By tuning the capacitance or inductance, we can shift this curve to the left or right, thereby tuning the reflection phase for a fixed frequency.

with little more than reactive tuning at the feed point. The separation limit is determined by the requirement that the capacitance between the antenna and the surface must be small compared to the built-in surface capacitance, so as not to detune the surface.

II. Tunable Impedance Surface

The resonance frequency of a textured ground plane can be tuned by adjusting the values of its effective circuit parameters L and C. Because the reflection phase is determined by the frequency of the incoming wave *with respect to the resonance frequency*, such a surface can perform as a distributed phase shifter. As the resonance frequency is swept from low to high, the curve in Fig. 2 is shifted from right to left, so the reflection phase at any fixed frequency varies from $-\pi$ to π. If the reflection phase is programmed as a function of position across the surface, it can be used for beam steering. A linear gradient $\partial\phi(x,y)/\partial x$ will reflect a normally incident microwave beam to an angle in the X-Z plane of

$$\theta = 2\tan^{-1}\left(\frac{\lambda}{2\pi}\frac{\partial\phi(x,y)}{\partial x}\right). \tag{4}$$

Other phase functions can be used for other tasks, such as a parabolic phase function for focusing. These concepts have been demonstrated previously using arrays of various resonant elements ranging from dipoles to patches, and beam-forming structures employing this technique are commonly known as reflectarrays [11]–[18]. Tunable reflectarrays using varactor diodes, [19], [20] and related devices known as grid arrays [21], [22] have also been built.

The resonance frequency and the reflection phase of a high-impedance surface can be tuned by changing the capacitance, the inductance, or both. However, the sheet inductance is given by

$$L = \mu t \tag{5}$$

where μ and t are the magnetic permeability and the thickness of the substrate. Without magnetically active materials, the inductance is primarily determined by the thickness, and is difficult to tune. The capacitance is easier to control by changing the geometry and arrangement of the metal plates, or by adding tunable lumped capacitors. Reflective beam steering using a mechanically tuned surface has already been demonstrated by adding

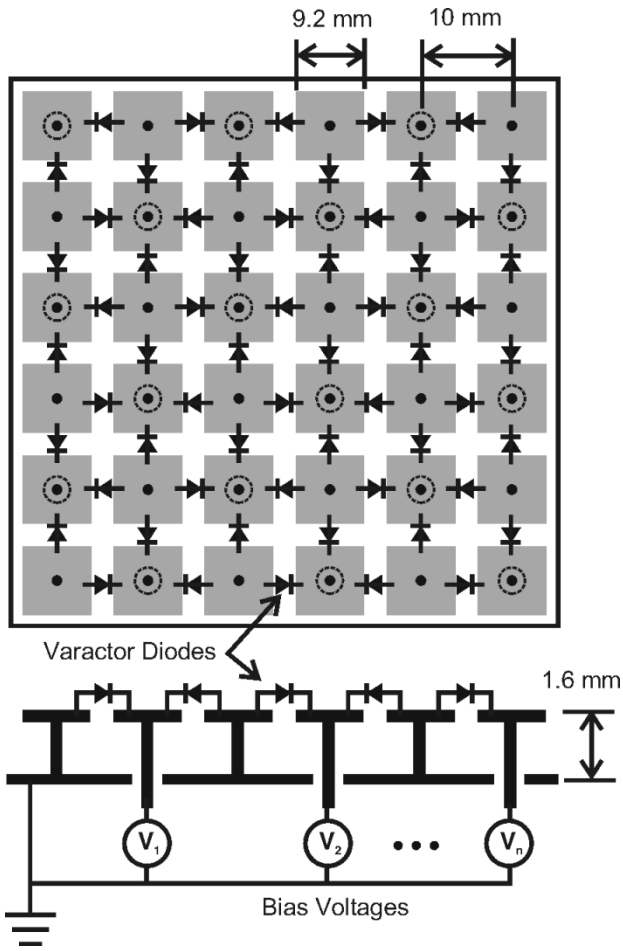

Fig. 3. Electrically tunable impedance surface, with varactor diodes between neighboring pairs of plates. Half of the plates are grounded, and the other half are attached to control wires on the back of the surface. The diodes are oriented in opposite directions in each alternate row.

a layer of movable tuning plates that overlap with a stationary high-impedance surface [23]. Moving the tuning layer with respect to the surface changes the resonance frequency, and rotating the tuning layer with respect to the stationary surface produces a phase gradient, which steers a reflected beam.

In our electrically tunable impedance surface, the movable plates are replaced with varactor diodes, as illustrated in Fig. 3. Each unit cell in the periodic surface texture is connected to its four neighbors by reverse-biased diodes. By changing the voltage on the diodes, we adjust the capacitance between neighboring cells, and tune the resonance frequency. In order to supply the required voltage to all of the varactors, we alternately bias half of the cells, and ground the other half in a checkerboard pattern. At the center of each biased cell, a metal via passes through a hole in the ground plane, and connects to a control line located on a separate circuit layer on the back of the surface. By controlling the varactors from the back of the surface in this way, the bias lines do not interfere with the microwave fields on the front side. The varactors are oriented in opposite directions in each alternate row, so that when a positive voltage is applied to control lines, all the diodes are reverse-biased. By individually addressing each cell, the reflection phase can be programmed as a function of position across the surface.

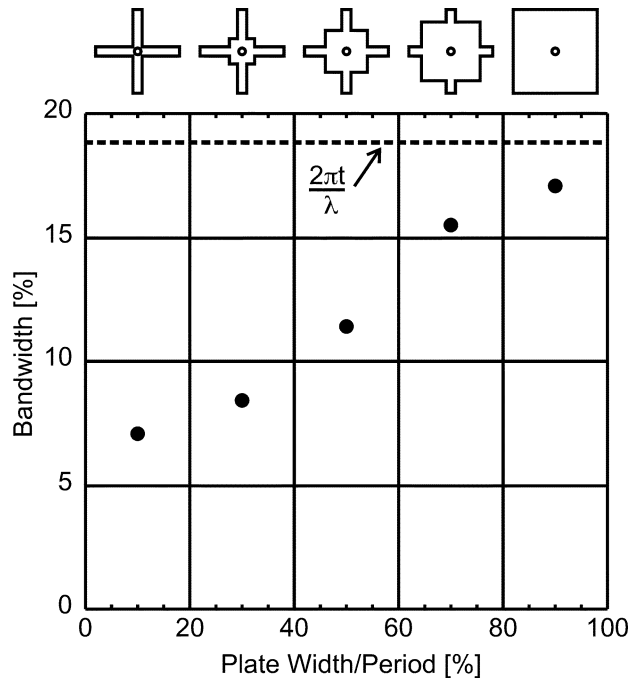

Fig. 4. Plot of the simulated bandwidth for various geometries, ranging from a thin wire grid to a lattice of broad plates. In each case, the period was 1 cm, and a 1-mm dielectric cube was placed at each edge to model the varactors. The theoretical bandwidth for a high-impedance surface with a thickness of 0.03λ is shown as a dashed line.

III. Bandwidth of Reflectarrays

It is known that the geometry of the resonant elements can have a significant effect on the performance of reflectarrays [16], [17], so we examined the effect of the plate geometry on the properties of our textured surface. For example, a thin wire grid structure has a greater tuning range than a broad plate structure because it has lower fixed capacitance. Related devices known as grid arrays have already demonstrated 1-D steering, using a series of metal strips printed on a grounded substrate, and connected by rows of varactors [21], [22].

We simulated a series of structures using Hewlett Packard High Frequency Structure Simulator (HFSS). In modeling these periodic surface textures, one unit cell is sufficient to determine the reflection phase. Typically, the single unit cell is placed at the end of a square TEM waveguide, which has electric boundaries on two opposing walls, and magnetic boundaries on the other two walls. A wave is excited from a port at the front end of the waveguide, and the reflection phase from the surface at the back end is recorded as a function of frequency. Although this method only provides the reflection phase for normal incidence, it is sufficient for examining trends in the reflection phase bandwidth with changes in geometry. We studied geometries ranging from simple squares to a narrow wire grid, shown in Fig. 4. For every case, the substrate was 1.6-mm-thick Rogers Duroid 5880. The lattice had a 1-cm period, and 1–mm dielectric cubes were centered on the plate edges to simulate the varactor diodes. By changing the dielectric constant in these small cubes, we could tune the reflection phase as a function of frequency.

By narrowing the square plates to a grid of wires, the fixed capacitance is reduced, and the tuning range is increased. However, the bandwidth is also diminished as shown in Fig. 5. We

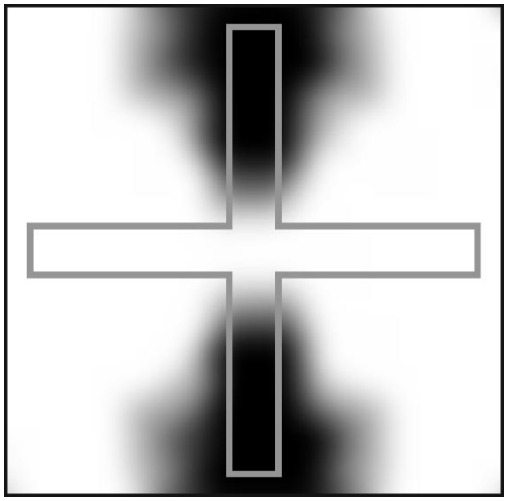

(a)

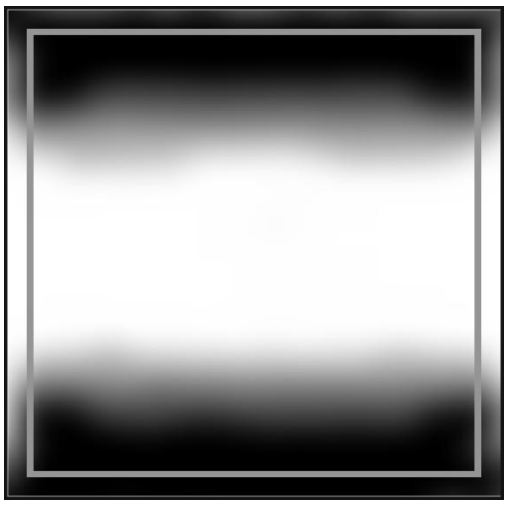

(b)

Fig. 5. Electric field within the substrate for two different plate geometries. (a) In a thin wire grid structure the electric field is primarily concentrated beneath the wires, which tends to reduce the bandwidth. (b) In a flat plate structure the field is more evenly distributed throughout the surface.

define the bandwidth of the resonance as the range where the phase falls between $+\pi/2$ and $-\pi/2$. This measure of bandwidth is directly proportional to its usable instantaneous bandwidth as a beam steering reflector, because a reflectarray with a steeper phase curve is less able form a consistent phase profile over a broad range of frequencies.

This dependence of the bandwidth on the plate geometry can be explained by examining the electric fields within the surface texture. The field inside the substrate is shown for two cases in Fig. 5. For the narrow wire grid structure, the electric field is primarily concentrated beneath the wires, while for the lattice of square plates, it is more evenly distributed across the plate edges. The field distribution within a resonant textured surface affects its bandwidth in much the same way as for a small resonant antenna, as first described by Wheeler and Chu [24]–[26]. A small antenna having a volume V is limited to a maximum bandwidth of

$$B \leq \frac{V}{V_0} \tag{6}$$

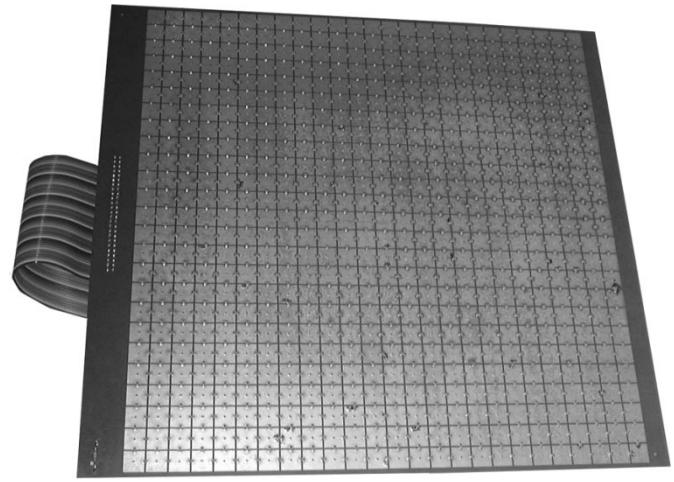

Fig. 6. Photograph of the electronically steerable reflector. The lattice period is 1 cm, and there are 25 × 25 cells. There are 1125 varactors, which are addressed in rows through the ribbon cable at the left edge. At 4.5 GHz, the surface is about 3.75-wavelengths wide.

where V_0 is the volume of a sphere having a radius of

$$r_0 = \frac{\lambda_0}{2\pi} \tag{7}$$

known as the radian length. The bandwidth is further reduced from this upper limit by the degree to which the fields do not uniformly fill that volume, so an antenna with highly localized fields tend to have narrower bandwidth. For a resonant textured ground plane, the same rule may be applied, and structures with uneven field distributions tend to have narrower bandwidths.

The theoretical bandwidth for a high impedance surface is indicated by a dashed line in Fig. 4. This bandwidth can be calculated as the frequency range where the magnitude of the surface impedance is greater than the impedance of free space

$$\left| \frac{j\omega L}{1 - \omega^2 LC} \right| > \eta. \tag{8}$$

We solve for ω to yield the frequencies of the two band edges

$$\omega^2 = \frac{1}{LC} + \frac{1}{2\eta^2 C^2} \pm \frac{1}{\eta C}\sqrt{\frac{1}{LC} + \frac{1}{4\eta^2 C^2}}. \tag{9}$$

The terms in $1/\eta^2\mathrm{C}^2$ are typically small compared to the terms in $1/\mathrm{LC}$, so we neglect them to obtain

$$\omega \approx \omega_0 \sqrt{1 \pm \frac{Z_0}{\eta}} \tag{10}$$

where

$$Z_0 = \sqrt{\frac{L}{C}}. \tag{11}$$

For structures that are thin compared to the wavelength, Z_0 is typically small compared to η, so we can expand the square root in (10), to approximate the fractional bandwidth as

$$\frac{\Delta\omega}{\omega_0} \approx \frac{Z_0}{\eta} = \frac{\sqrt{\frac{L}{C}}}{\sqrt{\frac{\mu_0}{\varepsilon_0}}}. \tag{12}$$

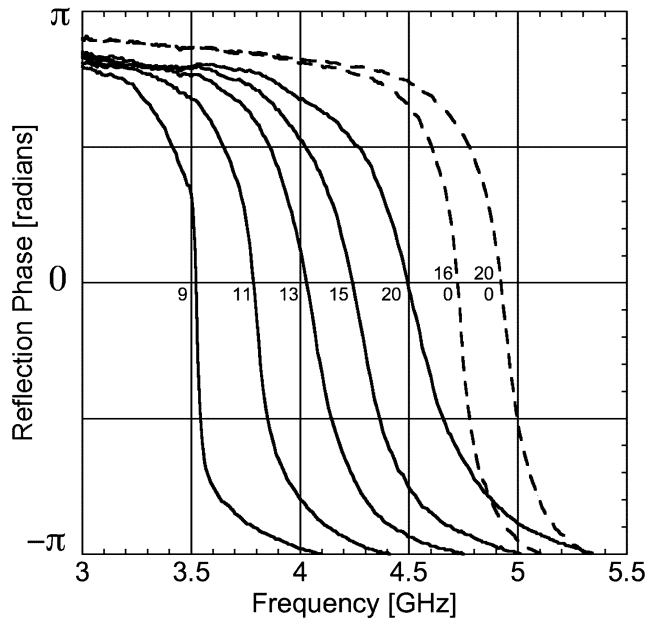

(a)

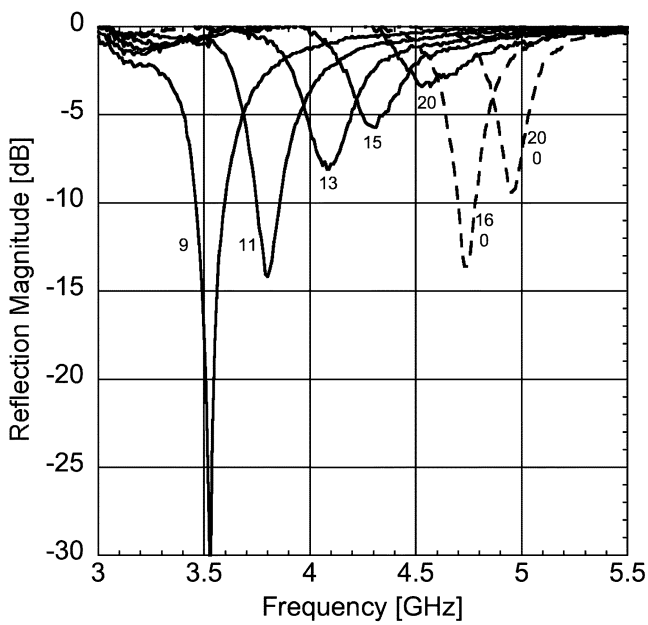

(b)

Fig. 7. (a) Reflection phase and (b) the magnitude for various voltages. The solid lines correspond to a uniform voltage ranging from 9 to 20 V, which provide a tuning range of 3.5 to 4.5 GHz. For the dashed lines, two different voltages were applied to alternate rows, which doubles the effective period, splitting the resonance in two, and pushing the upper resonance to nearly 5 GHz.

Using (2) and (5) we multiply the numerator and denominator by ω_0, and substitute for L to obtain

$$\frac{\Delta\omega}{\omega_0} \approx t\frac{2\pi}{\lambda_0} \tag{13}$$

where λ_0 is the free space wavelength at the resonance frequency. We recognize $\lambda_0/2\pi$ as the radian length in (7) [24]. Thus, the bandwidth B of a thin, ($\mathrm{t} \ll \lambda$) nonmagnetic, ($\mu = \mu_0$) resonant textured ground plane is limited by its thickness divided by the radian length at resonance. It is further reduced by the degree to which the fields are localized within the surface

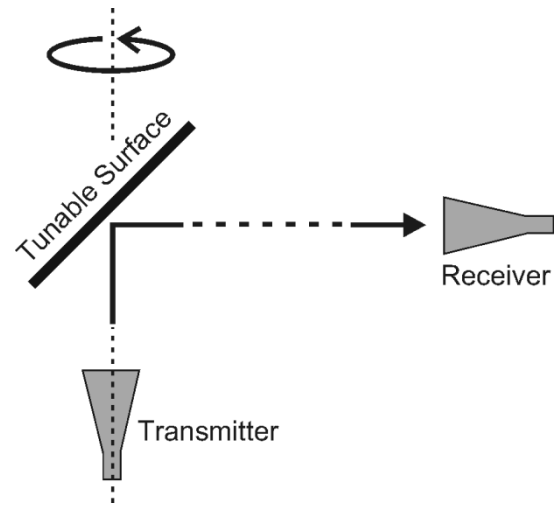

Fig. 8. Setup for measuring the radiation pattern of the tunable surface. It was oriented at 45° to the horizon, and illuminated from below by a feed horn. The surface and feed horn were rotated about the vertical axis, and the radiation pattern was measured in the horizontal plane by a second receive horn.

texture and do not uniformly fill its volume, as summarized by the inequality

$$B \leq \frac{t}{r_0} \tag{14}$$

which can be viewed as the 2-D analog of (6), derived here for a resonant textured surface.

One can further expect that any array of resonant elements where the period is significantly greater than the size of the elements would suffer a similar reduction in bandwidth, compared to a densely packed lattice, due to the unused portions of the surface area where the fields are negligible. Indeed, similar trends in bandwidth are seen for traditional reflectarrays [16], [17]. Furthermore, (14) only specifies the maximum inherent bandwidth of the resonant surface. Its usable bandwidth as a beam steering reflector is even less, because of the curvature of the reflection phase function

$$\frac{\partial\phi(x,y)}{\partial f} \neq 0 \tag{15}$$

and the need for 2π phase discontinuities to steer to large angles.

IV. Design and Characterization

We built our tunable impedance surface as a lattice of square plates with varactor diodes connecting between each adjacent pair of plates, as shown in Fig. 6. The diodes are Micrometrics silicon hyperabrupt varactors, model MHV500–19–1, which have a usable capacitance range of roughly 0.2 to 0.8 pF. From (2), we can expect a frequency tuning range of somewhat less than 2:1 with these varactors. The surface is built as a multilayer circuit board, with three metal layers and two substrate layers. The front metal layer contains the lattice of square plates, the middle layer is the ground plane, and the back layer contains the control lines that bias the varactors. The substrate layers are both 1.6-mm-thick Rogers Duroid 5880, and were designed with equal thickness to prevent warping of the substrate during fabrication. The square metal plates are 9.2-mm wide, and the

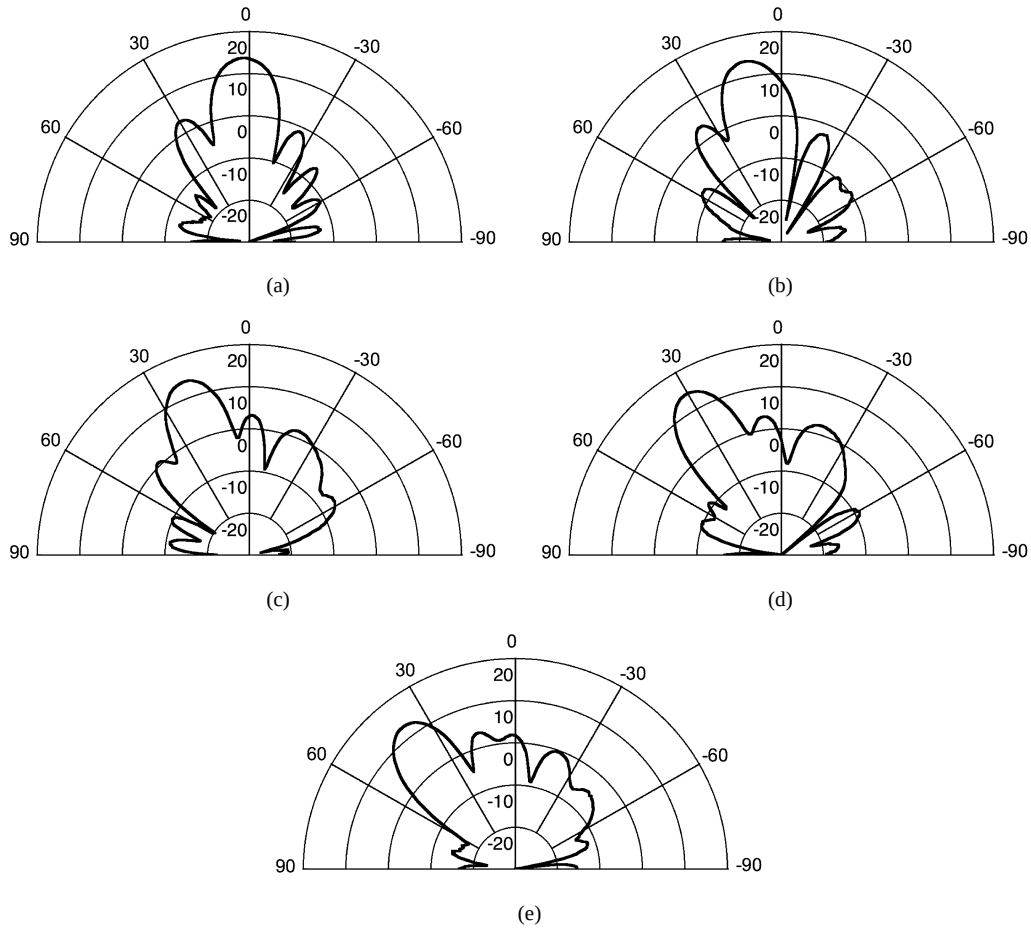

Fig. 9. For E-plane steering, the feed horn is oriented so that the electric field lies within the horizontal plane. The surface was programmed for (a) 0°, (b) 10°, (c) 20°, (d) 30°, and (e) 40°. It could also steer by an equal amount in the opposite direction.

period is 10 mm. The surface measures 25-cm square, for a total of 625 individual plates. It uses 1152 varactors, which were automatically attached using a pick-and-place machine.

We measured the reflection phase of the tunable surface as a function of bias voltage and frequency. A flat metal plate of the same size was used as a reference. In order to eliminate unwanted reflections from nearby objects and artifacts from the feed horn, the surface was oriented at 45° with respect to both the transmitter and the receiver. The phase and magnitude of the reflection coefficient are shown in Fig. 7 for various voltages. By tuning the voltage on the varactors from 0 to 20 V, the resonance frequency can be tuned over a range of about 2.5 to 4.5 GHz. However, the surface is only useful for beam steering above about 3.5 GHz because at lower bias voltages the varactors have greater loss, which diminishes the antenna gain and distorts the phase curve.

The solid lines in Fig. 7 correspond to a uniform voltage ranging from 9 to 20 V, which tunes the surface from 3.5 to 4.5 GHz. Higher resonance frequencies are achieved by alternating between two voltages on every other row. This effectively doubles the lattice period and splits the resonance into two separate modes as the Brillouin zone [27] is folded in upon itself. The formation of a second mode allows the surface to be tuned as high as 5 GHz, as shown by the dashed lines. This also has important effects on the surface wave band structure, but that topic is beyond the scope of the present discussion.

V. Reflective Beam Steering

A series of reflection phase curves, like those shown in Fig. 7, serves as a calibration table that is used to program the surface for reflective beam steering. To steer to a given angle, we calculate the required reflection phase gradient using (4), then select a frequency, and calculate the corresponding voltages for each bias line from the calibration table. The process of calibration and steering was automated using National Instruments Labview software. This straightforward method can produce measurable beam steering [28], but it does not take into account the phase curvature of the feed horn, and is susceptible to calibration errors and manufacturing variations in the surface and the varactors. We mitigated these effects by using a simple algorithm to optimize the bias voltages: the surface was rotated to the desired angle, and the received power was monitored as the voltage on each bias line was dithered by successively smaller values, until the received power did not change. The radiation pattern for each selected steering angle was then measured using these optimized voltages.

To measure the beam steering capabilities of the surface, it was suspended 25 cm above a vertical feed horn, at 45° to the horizon, as illustrated in Fig. 8. The surface and horn are mounted on a rotating pedestal in an anechoic chamber. Radiation from the feed horn reflects from the surface, and is received by a separate receiving horn. By rotating the feed horn and the

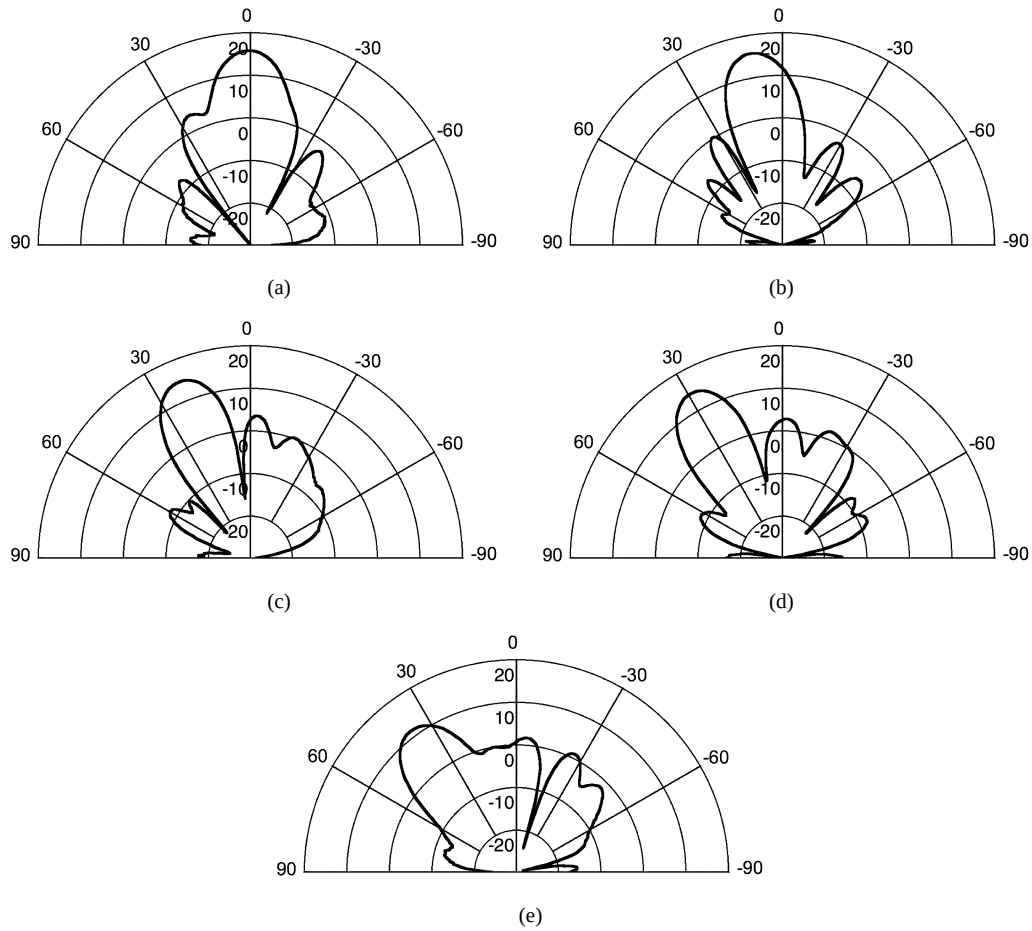

Fig. 10. For H-plane steering, the feed horn is oriented so that the magnetic field lies within the horizontal plane. The surface was programmed for (a) 0°, (b) 10°, (c) 20°, (d) 30°, and (e) 40°. It could also steer by an equal amount in the opposite direction.

surface, we measure the radiation pattern in the horizontal plane. This arrangement prevents unwanted reflections and extraneous radiation from the feed horn from interfering with the measurement, because they are absorbed by the ceiling or floor of the anechoic chamber. The experiment was also simplified by addressing the cells in rows, so the reflected beam was only steered in the horizontal plane. By showing 1-D steering for two polarizations, we demonstrate the capability of 2-D steering, because the surface has fourfold rotational symmetry. Full 2-D steering would require each cell to be addressed individually, or scanned using a row-and-column addressing scheme.

The radiation patterns were measured for each set of control voltages corresponding to several steering angles. For E-plane steering, shown in Fig. 9, the feed horn is positioned so that the electric field projected on the surface is oriented within the horizontal plane. For H-plane steering, shown in Fig. 10, the feed horn is rotated by 90°. We found that the surface could steer a reflected beam over $+/-40°$ for both polarizations. The measurements shown are for 4.5 GHz, but the radiation pattern could be optimized over a broad range of frequencies within the tuning range of the surface.

VI. Performance Summary

The electronically steerable reflector had an average gain of about 14 dBi, and an average beamwidth of about 15°, as seen in Figs. 9 and 10. The first sidelobes had an average magnitude of − 15 dB with respect to the main beam. However, the left and right sidelobes typically had different values, and the greater of the two was − 10 dB on average. An ideal radiator of this size with 100% efficient uniform illumination would have a gain of 21 dBi, a beamwidth of 14°, and − 13 dB sidelobes. Thus, the tunable reflector produces a nearly ideal pattern shape, but the measured gain is 7 dB less than ideal due to a combination of material loss, spillover, and phase errors.

To quantify the intrinsic efficiency of the tunable surface, we measured the radiation pattern for a flat metal sheet of the same size, which is shown in Fig. 11. The metal reflector had a gain of 14 dBi, and a beamwidth of 20°. The sidelobes appear as shoulders on the main beam, at an average level of about − 7 dB. Our tunable reflector had a narrower beamwidth than the metal reflector because our adaptive algorithm for optimizing the control voltages introduced curvature into the phase function, which provided focusing. By integrating the pattern of the metal surface, we estimate that the spillover efficiency is 46%, accounting for 3.4 dB of the measured discrepancy from an ideal reflector. This factor primarily depends on the design of the feed horn.

By integrating the radiation pattern for the tunable surface at the 0° scan angle, we find a total efficiency of 30%. Assuming the same spillover loss as the metal sheet, the tunable surface can

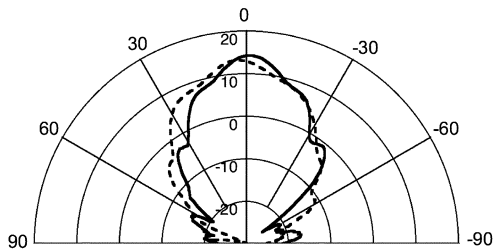

Fig. 11. Radiation pattern for a flat metal reflector was measured to determine the efficiency of the tunable surface. The E-plane pattern is shown as a solid line, and the H-plane pattern is shown as a dashed line.

TABLE I
PERFORMANCE SUMMARY FOR THE ELECTRONICALLY STEERABLE REFLECTOR, COMPARED TO MEASUREMENTS OF A FLAT METAL SURFACE, AND AN IDEAL SURFACE WITH UNIFORM ILLUMINATION

	tunable surface	metal plate	ideal
gain	14 dB	14 dB	21 dB
beamwidth	15 degrees	20 degrees	14 degrees
spillover efficiency	46%	46%	100%
reflection efficiency	65%	100%	100%
total efficiency	30%	46%	100%
average sidelobes	-15 dB	-7 dB	-13 dB
maximum sidelobes	-10 dB	-6 dB	-13 dB
squint	0.02 degrees/MHz	–	0.004 degrees/MHz
bandwidth	8%	–	–

be assigned a reflection efficiency of 65%, representing about 1.9 dB of loss. This could be improved by using GaAs varactors, which typically have lower loss, or by using a thicker surface, which would have a broader bandwidth. In general, the reflection loss of a resonant textured surface is proportional to the loss in its constituent materials divided by its bandwidth

$$\mathrm{Loss}_{\mathrm{Surface}} \propto \frac{\mathrm{Loss}_{\mathrm{Material}}}{B}. \tag{16}$$

This is because structures with narrower bandwidth tend to have higher electric field intensities within the dielectric regions, and greater current densities within the conductive regions. Conversely, the bandwidth of a resonant structure can be increased by adding loss, although this is generally not desirable.

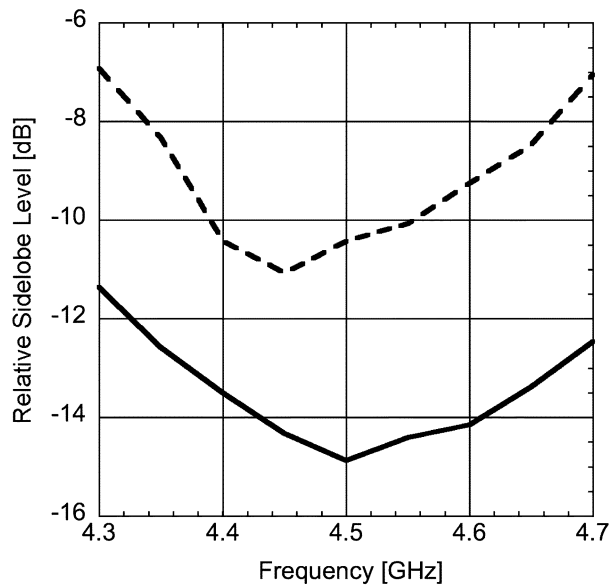

Fig. 12. Average value of the first left and right sidelobes is plotted as a solid line, and the higher of the two is plotted as a dashed line, as a function of frequency. The data is averaged over $+/-40°$ scan angles. The surface was optimized for 4.5 GHz. The sidelobes degrade by 3 dB within a bandwidth of about 8%.

The remaining 1.7 dB reduction in the main beam compared to an ideal reflector is likely due to phase errors, which tend to direct more energy into sidelobes. This could be improved with more careful calibration and optimization of the control voltages. The performance of the tunable reflector is summarized, compared to the metal surface and an ideal reflector in Table I.

The gain and beamwidth did not vary significantly with frequency, so they are poor measures of the antenna bandwidth. Therefore, we choose to quantify the bandwidth using two parameters that are more sensitive: beam squint, and sidelobe variation. By optimizing the surface for 4.5 GHz, and then examining the radiation patterns at other frequencies, we found that the peak direction of the main beam varied by about 0.02°/MHz on average. Using this measure, the instantaneous bandwidth of the antenna is limited by the beamwidth required. For example, a 100 MHz signal would have a minimum beamwidth of 2°. From (4), we find that the ideal average variation would be 0.004°/MHz over a $+/-40°$ scan if the reflection phase were independent of frequency. To reduce the squint below this level would require true time delay, rather than phase control. The difference between our measurement and the ideal case is due to the frequency dependence of the phase function, and could be improved by using a thicker surface.

We can also quantify the bandwidth from the variation in the sidelobe levels. In Fig. 12, the surface was optimized for 4.5 GHz, and we plot the average and maximum sidelobe levels for various frequencies. If we define the bandwidth as the frequency range where the sidelobes are degraded by 3 dB, this surface has a bandwidth of about 8%. As with the beam squint, this would be greater for a thicker structure, in which the phase curve would have a broader natural bandwidth.

VII. Conclusion

We have described an electronically steerable reflector, based on a resonant textured surface loaded with varactor diodes. By varying the bias voltage across the varactors, we can change the reflection phase of the surface as a function of frequency. We can program the reflection phase across the surface to produce a tunable phase gradient, which can steer a reflected microwave beam. We have demonstrated 2-D beam steering over a range of $+/-40^\circ$ for both polarizations. We have also analyzed the bandwidth for these and similar surfaces. This analysis suggests that structures where the field distribution is the most uniform tend to have the broadest bandwidth, and that the bandwidth is ultimately limited by the thickness. The surface used in our experiments has a bandwidth of about 8%, which is sufficient for many modern communication requirements. Because it consists of nothing more than printed circuit boards and varactors, this electronically steerable antenna could serve as a low-cost substitute for many conventional phased arrays.

Acknowledgment

The authors would like to thank M. Musni for help with the fabrication of the surface.

References

[1] P.-S. Kildal, "Artificially soft and hard surfaces in electromagnetics," *IEEE Trans. Antennas Propagat.*, vol. 38, pp. 1537–1544, June 1990.
[2] A. Harvey, "Periodic and guiding structures at microwave frequencies," *IRE Trans.*, vol. 8, p. 30, 1959.
[3] C. Elachi, "Waves in active and passive periodic structures: A review," *Proc. IEEE*, vol. 64, p. 1666, 1976.
[4] L. Brillouin, "Wave guides for slow waves," *J. Appl. Phys.*, vol. 19, p. 1023, 1948.
[5] W. Rotman, "A study of single-surface corrugated guides," *Proc. IRE*, vol. 39, p. 952, 1951.
[6] R. Elliot, "On the theory of corrugated plane surfaces," *IRE Trans. Antennas Propagat.*, vol. 2, p. 71, 1954.
[7] S. Lee and W. Jones, "Surface waves on two-dimensional corrugated surfaces," *Radio Sci.*, vol. 6, p. 811, 1971.
[8] R. King, D. Thiel, and K. Park, "The synthesis of surface reactance using an artificial dielectric," *IEEE Trans. Antennas Propagat.*, vol. 31, pp. 471–476, May 1983.
[9] D. Sievenpiper, "High-impedance electromagnetic surfaces," Ph.D. dissertation, Univ. California, Dept. Elect. Eng., Los Angeles, CA, 1999.
[10] D. Sievenpiper, L. Zhang, R. Broas, N. Alexopolous, and E. Yablonovitch, "High-impedance electromagnetic surfaces with a forbidden frequency band," *IEEE Trans. Microwave Theory Tech.*, vol. 47, pp. 2059–2074, Nov. 1999.
[11] D. G. Berry, R. G. Malech, and W. A. Kennedy, "The reflectarray antenna," *IEEE Trans. Antennas Propagat.*, vol. 11, pp. 645–651, Nov. 1963.
[12] Y.-L. Chen and Y. Lo, "Reactive reflectors," *IEE Proc.*, vol. H 131, p. 263, 1984.
[13] J. Huang, "Reflectarray antenna," in *Proc. IEEE Antennas Propagation Soc. Int. Symp. Dig.*, 1991, pp. 612–615.
[14] R. D. Javor, X.-D. Wu, and K. Chang, "Design and performance of a microstrip reflectarray antenna," *IEEE Trans. Antennas Propagat.*, vol. 43, pp. 932–939, Nov. 1995.
[15] D. C. Chang and M. C. Huang, "Multiple polarization microstrip reflectarray antenna with high efficiency and low cross-polarization," *IEEE Trans. Antennas Propagat.*, vol. 43, pp. 829–834, Aug. 1995.
[16] D. M. Pozar, S. D. Targonski, and H. D. Syrigos, "Design of millimeter wave microstrip reflectarrays," *IEEE Trans. Antennas Propagat.*, vol. 45, pp. 187–296, Feb. 1997.
[17] K. Y. Sze and L. Shafai, "Substrate thickness in a microstrip reflectarray," in *Proc. Asia Pacific Microwave Conf.*, vol. 1, 1999, pp. 146–149.
[18] M. E. Bialkowski and H. J. Song, "Investigations into a power combining structure using a reflect array of dual-feed aperture coupled microstrip patch antennas," *IEEE Trans. Antennas Propagat.*, vol. 50, pp. 841–849, June 2002.
[19] R. Waterhouse and N. Shuley, "Scan performance of infinite arrays of microstrip patch elements loaded with varactor diodes," *IEEE Trans. Antennas Propagat.*, vol. 41, pp. 1273–1280, Sept. 1993.
[20] L. Boccia, F. Venneri, G. Amendola, and G. Di Massa, "Application of varactor diodes for reflectarray phase control," in *Proc. IEEE Antennas Propagat. Soc. Int. Symp.*, vol. 3, 2002, pp. 132–135.
[21] W. Lam, C. Jou, H. Chen, K. Stolt, N. Luhmann, and D. Rutledge, "Millimeter wave diode grid phase shifters," *IEEE Trans. Microwave Theory Tech.*, vol. 36, pp. 902–907, May 1988.
[22] L. B. Sjogren, H. X. Liu, X. Qin, C. W. Domier, and N. C. Luhmann, "Phased array operation of a diode grid impedance surface," *IEEE Trans. Antennas Propagat.*, vol. 42, pp. 565–572, Apr. 1994.
[23] D. Sievenpiper, J. Schaffner, R. Loo, G. Tangonan, S. Ontiveros, and R. Harold, "A tunable impedance surface performing as a reconfigurable beam steering reflector," *IEEE Trans. Antennas Propagat.*, vol. 50, pp. 384–390, Mar. 2002.
[24] H. Wheeler, "Fundamental limitations of small antennas," *Proc. IRE*, vol. 35, p. 1479, 1947.
[25] L. Chu, "Physical limitations of Omni-directional antennas," *J. Appl. Phys.*, vol. 19, p. 1163, 1948.
[26] J. McLean, "A re-examination of the fundamental limits on the radiation Q of electrically small antennas," *IEEE Trans. Antennas Propagat.*, vol. 44, p. 672, May 1996.
[27] L. Brillouin, *Wave Propagation in Periodic Structures*: McGraw-Hill, 1946.
[28] D. Sievenpiper and J. Schaffner, "Advances in electronic beam steering using electronically tunable impedance surfaces," *IEEE APS Symp. Dig.*, vol. 4, p. 262, 2002.

Daniel F. Sievenpiper (S'95–M'98) received the B.S. and Ph.D. degrees in electrical engineering from the University of California, Los Angeles, in 1994 and 1999, respectively, where he studied microwave photonic crystals, and developed high impedance textured ground planes for low profile antennas.

He is currently a Senior Research Staff Engineer with the Communications and Photonics Lab, HRL Laboratories, where he is working in the field of wireless communication and antennas. His interests include advanced radio architectures, tunable antennas, low cost beam steering techniques, and novel electromagnetic materials. He holds 10 U.S. patents, 15 refereed journal publications, and 26 conference papers and other publications.

James H. Schaffner (S'74–M'79–SM'97) received the B.S., M.S., and Ph.D. degrees in electrical engineering from the University of California, Los Angeles, in 1978, 1979, and 1988, respectively.

He is a Senior Research Scientist with HRL Laboratories, where he has worked since 1988. He was the program manager for HRL's DARPA RECAP program. From 1978 to 1988, he was with the Hughes Aircraft Company Missile System Group, where he worked on microwave and millimeter wave antenna arrays, antenna feed networks, and MMIC circuits for transmit/receive modules. His current research interests are components, systems, and metrology for optical and millimeter wave broadband communications channels.

H. Jae Song (S'95–M'01) received the B.E., M.Eng.Sc., and Ph.D. degrees in electrical engineering from the University of Queensland, Australia, in 1995, 1998, and 2001, respectively.

He is a Research Staff Member in the Communications and Photonics Lab at HRL Laboratories. Since he joined HRL Laboratories, he has been mainly working on various antenna projects. His primary research interests are passive and active microstrip patch array antennas and RF/microwave circuits for wireless communication applications. His other research interests include quasi-optical/spatial power-combining techniques and amplifiers. He is a coauthor of two book chapters and more than 30 published journal/conference papers in the fields of antennas and spatial power combining techniques.

Robert Y. Loo (M'02) received the Ph.D. degree in electrical engineering from the University of California, Los Angeles, in 1976.

He is the Chief Technology Officer at Wireless MEMS Incorporated, Oak Park, CA. Before joining Wireless MEMS Incorporated in 2003, he was a Principal Research Scientist, Manager of Communication Networks Department, and Leader of the RF MEMS Technology team at HRL Laboratories (formerly known as Hughes Research Laboratories). He joined Hughes in 1976 and has been responsible for the development of GaAs solar cell technology, and he developed a model that improved the radiation resistance of the cell. During recent years, he has been developing low loss and high isolation metal contact RF MEMS switches and circuits for microwave and antenna applications. He also has been working on high-speed InGaAs–InP PIN photodetector arrays and optoelectronic selector switches for the phased array antenna and WDM optical networks for subcarrier multiplexing signal applications. He has 30 years experience in semiconductor materials and photonic device technology. He has coauthored 35 technical papers on semiconductor devices, optical control of phased arrays, GaAs solar cells, and RF MEMS.

Gregory Tangonan (M'94) joined Hughes Research Laboratories in 1971 after receiving the Howard Hughes Doctoral Fellowship for studies at the California Institute of Technology, Pasadena. He has contributed to the development of integrated waveguide detectors, Bragg modulators in $LiTaO_3$ and $LiNbO_3$, waveguide couplers for WDM systems, and all-optical networking techniques for analog and digital signals. In 1994, he was promoted to Laboratory Director of the Communications and Photonics Laboratory (CPL), reporting to the President of HRL Laboratories. CPL focused on communications applications of high power lasers, fiber laser, RF photonics and mobile wireless access. In wireless access CPL, research thrusts include Hybrid laser/mmwave wireless communications and reconfigurable analog front-ends, diversity antennas, and RF MEMS circuits for mobile wireless access. After 31 years with HRL Laboratories, he retired from HRL Laboratories to pursue new interests. He joined the Ateneo de Manila University, Philippines, as Professor in the Loyola School of Science and Engineering. He is coauthor of more than 120 published papers and presentations in the fields of fiber optics, RF photonics, and wireless access technologies. He has 38 U.S. patents.

Dr. Tangonan is a Member of the Optical Society of America, the IEEE Lasers and Electro-Optics Society, and Sigma Xi. He is the recipient of two R&D 100 Awards for the development of innovative fiber optic products.